

Helicity-dependent photoconductance of the edge states in the topological insulator Bi_2Te_3

Yuchao Zhou(周宇超), Jinling Yu(俞金玲), Yonghai Chen(陈涌海),Yunfeng Lai(赖云锋), and Shuying Cheng(程树英)

Citation: Chin. Phys. B, 2023, 32 (**8**): 087102. DOI: 10.1088/1674-1056/acc3fb
Journal homepage: http://cpb.iphy.ac.cn; http://iopscience.iop.org/cpb

What follows is a list of articles you may be interested in

Topological properties of tetratomic Su-Schrieffer-Heeger chains with hierarchical long-range hopping

Guan-Qiang Li(李冠强), Bo-Han Wang(王博涵), Jing-Yu Tang(唐劲羽), Ping Peng(彭娉), and Liang-Wei Dong(董亮伟)

Chin. Phys. B, 2023, 32 (**7**): 077102. DOI: 10.1088/1674-1056/aca7ef

Coexistence of giant Rashba spin splitting and quantum spin Hall effect in H-Pb-F

Wenming Xue(薛文明), Jin Li(李金), Chaoyu He(何朝宇), Tao Ouyang(欧阳滔), Xiongying Dai(戴雄英), and Jianxin Zhong(钟建新)

Chin. Phys. B, 2023, 32 (**3**): 037101. DOI: 10.1088/1674-1056/aca7eb

Quantum anomalous Hall effect in twisted bilayer graphene quasicrystal

Zedong Li(李泽东) and Z F Wang(王征飞)†

Chin. Phys. B, 2020, 29 (**10**): 107101. DOI: 10.1088/1674-1056/abab77

Graphene-like Be_3X_2 (X=C, Si, Ge, Sn): A new family of two-dimensional topological insulators

Lingling Song(宋玲玲), Lizhi Zhang(张礼智), Yurou Guan(官雨柔), Jianchen Lu(卢建臣), Cuixia Yan(闫翠霞), Jinming Cai(蔡金明)

Chin. Phys. B, 2019, 28 (**3**): 037101. DOI: 10.1088/1674-1056/28/3/037101

Antiferromagnetic–ferromagnetic transition in zigzag graphene nanoribbons induced by substitutional doping

Shenyuan Yang(杨身园), Jing Li(李静), Shu-Shen Li(李树深)

Chin. Phys. B, 2018, 27 (**11**): 117102. DOI: 10.1088/1674-1056/27/11/117102

Helicity-dependent photoconductance of the edge states in the topological insulator Bi_2Te_3

Yuchao Zhou(周宇超)[1], Jinling Yu(俞金玲)[1,†], Yonghai Chen(陈涌海)[2,3], Yunfeng Lai(赖云锋)[1], and Shuying Cheng(程树英)[1,4]

[1] *Institute of Micro/Nano Devices and Solar Cells, School of Physics and Information Engineering, Fuzhou University, Fuzhou* 350108, *China*
[2] *Key Laboratory of Semiconductor Materials Science, Institute of Semiconductors, Chinese Academy of Sciences, Beijing* 100083, *China*
[3] *College of Materials Science and Opto-Electronic Technology, University of Chinese Academy of Sciences, Beijing* 100049, *China*
[4] *Jiangsu Collaborative Innovation Center of Photovolatic Science and Engineering, Changzhou University, Changzhou* 213164, *China*

(Received 19 January 2023; revised manuscript received 4 March 2023; accepted manuscript online 14 March 2023)

The helicity-dependent photoconductance of the edge states in three-dimensional topological insulator Bi_2Te_3 films is investigated. It is revealed that the helicity-dependent photoconductivity current on the left edge of the Bi_2Te_3 film shows an opposite sign with that on the right edge. In addition, the helicity-dependent photoconductivity current increases linearly with the applied longitudinal electric field, and it reverses the sign with the reversal of the electric field. As the thickness of the Bi_2Te_3 film increases, the helicity-dependent photoconductivity current also increases. Theoretical analysis suggests that the helicity-dependent photo-conductivity current may come from the intrinsic spin orbit coupling (SOC) or the SOC introduced by the chiral impurities or defects.

Keywords: helicity-dependent photoconductance, Bi_2Te_3, edge states, spin orbit coupling

PACS: 71.70.Ej, 72.25.Fe, 75.70.Tj, 75.76.+j **DOI:** 10.1088/1674-1056/acc3fb

1. Introduction

Three-dimensional (3D) topological insulators (TIs), as a new quantum phase of mater, are characterized by gapless spin-textured surface states that reside within the bulk band gap.[1–6] The electrons on the surface states of 3D TIs behave as Dirac fermions bearing a characteristic called spin-momentum locking. The unique properties of topological surface states make them promising in the field of spintronic devices and quantum computing.[7] Among the mangy 3D TIs, Bi_2Te_3 is a simple model with a single Dirac cone on the surface and relatively large bulk band gap (about 0.3 eV).[8]

In the past few years, there were many experimental works studying the surface states of 3D TIs, including investigations using time-resolved angle-resolved photo-emission spectroscopy (ARPES),[9,10] magnetotransport,[11,12] spin pumping,[13,14] and helicity-dependent photocurrent.[15–17] However, most of the works were focus on the top and bottom surface states, and very few of them investigated the edge states of 3D TIs.[16] As a result, lots of properties of the edge states of 3D TIs are still unknown. Recently, helicity-dependent photo-conductance has emerging as a powerful tool to investigate the spin Hall effect of edge states in Bi_2Te_2Se[16] and the current-induced spin polarization in Bi_2Te_3.[18] In addition, the helicity-dependent photo-conductance can also be used to investigate the intrinsic spin orbit coupling (SOC) or the SOC introduced by the chiral impurities or defects.[18] By measuring the helicity-dependent photo-conductance when the light is illuminated on the left and right edges, respectively, the signal of the left and right edges can be clearly identified. This has obvious advantages compared with that of the top and bottom surface states, since generally it is difficult to distinguish the signal of the top and bottom surface states.

In this paper, we investigate the helicity-dependent photoconductance of the edge states in three-dimensional topological insulator Bi_2Te_3 films with different thicknesses. It is found that the helicity-dependent photo-conductivity current (HDPC) on the left edge of the Bi_2Te_3 film shows an opposite sign with that on the right edge. The HDPC on the edge of the Bi_2Te_3 film almost increases linearly with the external applied longitudinal electric field. With the reversal of the electric field, the sign of the HDPC also reverses. Moreover, the HDPC on the edge of the Bi_2Te_3 film increases as the thickness of Bi_2Te_3 film increases. We find that the HDPC on the edge of the Bi_2Te_3 films may come from the intrinsic spin orbit coupling (SOC) or the SOC due to the chiral impurities or defects by using theoretical analysis.

2. Experimental details

The Bi_2Te_3 films with thicknesses of 5, 7, 12 and 20 quintuple (QL) investigated in this work are grown on insulating Si (111) substrates by molecular beam epitaxy (MBE). A pair of 10 nm Ti/100 nm Au strip contacts of 2×0.5 mm^2 with distance of 10 mm is deposited on the surface of Bi_2Te_3 by electron beam evaporation, as shown in Fig. 1(a). To prevent the degradation of the sample in air, the samples are mounted

†Corresponding author. E-mail: jlyu@semi.ac.cn

© 2023 Chinese Physical Society and IOP Publishing Ltd

on an optical cryostat with 1 Pa low-pressure chamber after bonding in air.

A diode-pumped solid-state laser with a wavelength of 1064 nm and a semiconductor laser of 1342 nm are used as the radiation source. After passing through a polarizer, a quarter-wave plate or a photoelastic modulator (PEM) and a lens with a focus of 200 mm, the laser irradiates on the sample with a light spot of a radius about 150 μm vertically. By using the PEM or rotating the quarter-wave plate, the helicity of the light can be modulated from right-handed circularly polarized to linearly polarized, to left-handed circularly polarized, periodically. A longitudinal electric field is applied by the two strip contacts, and the photocurrent is collected by the same contacts with a pre-amplifier and a lock-in amplifier.

When a quarter-wave plate is used, the light spot is illuminated normally at the left edge, the center, and the right edge of the Bi_2Te_3 film, denoted as points A, B, and C, respectively, as shown in Fig. 1(a). A chopper is used, and the reference frequency of the lock-in amplifier comes from the chopper with a working frequency of 229 Hz. The distance between points A, B, C and the two contacts are the same, thus the influence of the thermoelectric effect can be eliminated. Moreover, to investigate the dependence of the HDPC on the light spot positions, the PEM is adopted to replace the quarter-wave plate, and the light spot is moving from the left edge to the right edge of the Bi_2Te_3 film. When a PEM is adopted, the reference frequency of the lock-in amplifier comes from the first-order frequency of the PEM, i.e., 50 KHz. To measure the photoconductivity (PC) current, a chopper with a working frequency of 229 Hz is adopted. The PC current is measured by applying a DC bias on the two contacts, and collecting the photocurrent in the same contacts. The PC current is amplified by a pre-amplifier and a lock-in amplifier with the reference frequency coming from the chopper.

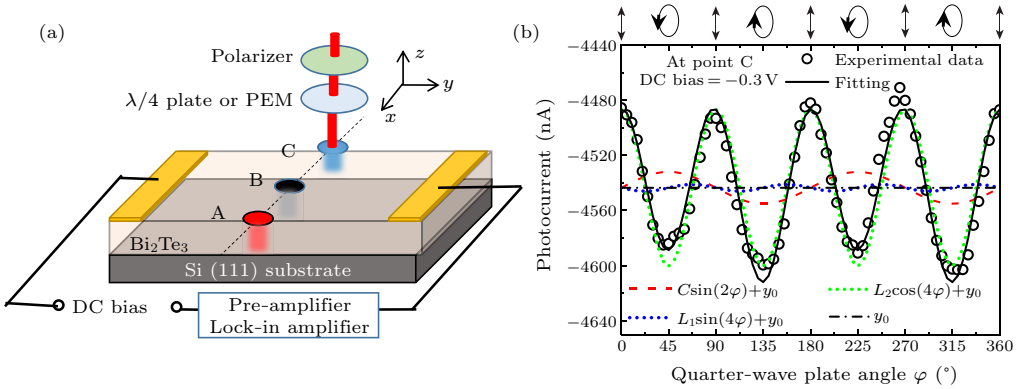


Fig. 1. (a) Schematic diagram of experimental setup of the HDPC current measurements. (b) Typical photocurrent as a function of quarter-wave plate angle under a DC bias of −0.3 V, when the laser is normally illuminated at point C of 20-QL Bi_2Te_3 film, as shown in panel (a). The solid line is the fitting curve by using Eq. (1), and the red dashed line indicates the $C\sin(2\varphi)+y_0$ component obtained by fitting. The blue dotted and green dotted lines are the $L_1\sin(4\varphi)+y_0$ and $L_2\cos(4\varphi)+y_0$ components, respectively.

3. Results and discussion

Figure 1(b) shows the typical photocurrent as a function of quarter-wave plate angle φ, when an external DC bias of −0.3 V is applied and the laser is normally illuminated on the right edge of the 20-QL Bi_2Te_3 film, i.e., point C as indicated in Fig. 1(a). The power of the 1064 nm laser on the sample is 45 mW. Here, φ is the angle between the polarization direction of the incident light and the optical axis of the quarter-wave plate. By fitting the light polarization state dependent photocurrent to the following equation, we can determine the HDPC current as follows:[15,19,20]

$$J = C\sin(2\varphi) + L_1\sin(4\varphi) + L_2\cos(4\varphi) + y_0. \quad (1)$$

Here, C is the amplitude of HDPC current. L_1 and L_2 are the amplitude of the photocurrent related to the linear photogalvanic effect (LPGE) or photon drag effect.[21] y_0 is the background current caused by photovoltaic effect, thermoelectric effect or Dember effect.[20,22] The solid line in Fig. 1(b) is the fitting result by using Eq. (1). It can be seen that the experimental data can be well fitted by Eq. (1). The red dashed line is the $C\sin(2\varphi)+J_0$ component obtained by fitting. The dotted blue and dotted green lines indicate the $L_1\sin(4\varphi)+y_0$ and $L_2\cos(4\varphi)+y_0$ components, respectively.

Figures 2(a)–2(c) show the HDPC current of the 20-QL sample under different DC biases as a function of the quarter-wave plate angle, i.e., $C\sin(2\varphi)$ component obtained by fitting of Eq. (1) to the experimental data, when the laser is normally illuminated at points A, B, and C, respectively. The light spot on the sample is Gaussian spot with a wavelength of 1064 nm of 45 mW. It can be seen that all the HDPC currents at point A, B, and C reverse the sign with the reversal of the DC bias. In addition, the HDPC current at the edge, i.e., points A and C, of the Bi_2Te_3 film is much larger than that at the center of the film, i.e., point B. The reasons for this phenomenon will be discussed later. Figure 2(d) shows the HDPC current under a DC bias of −0.3 V, i.e., $C\sin(2\varphi)$ component, as a function of the quarter-wave plate angle, when the laser is illuminated at

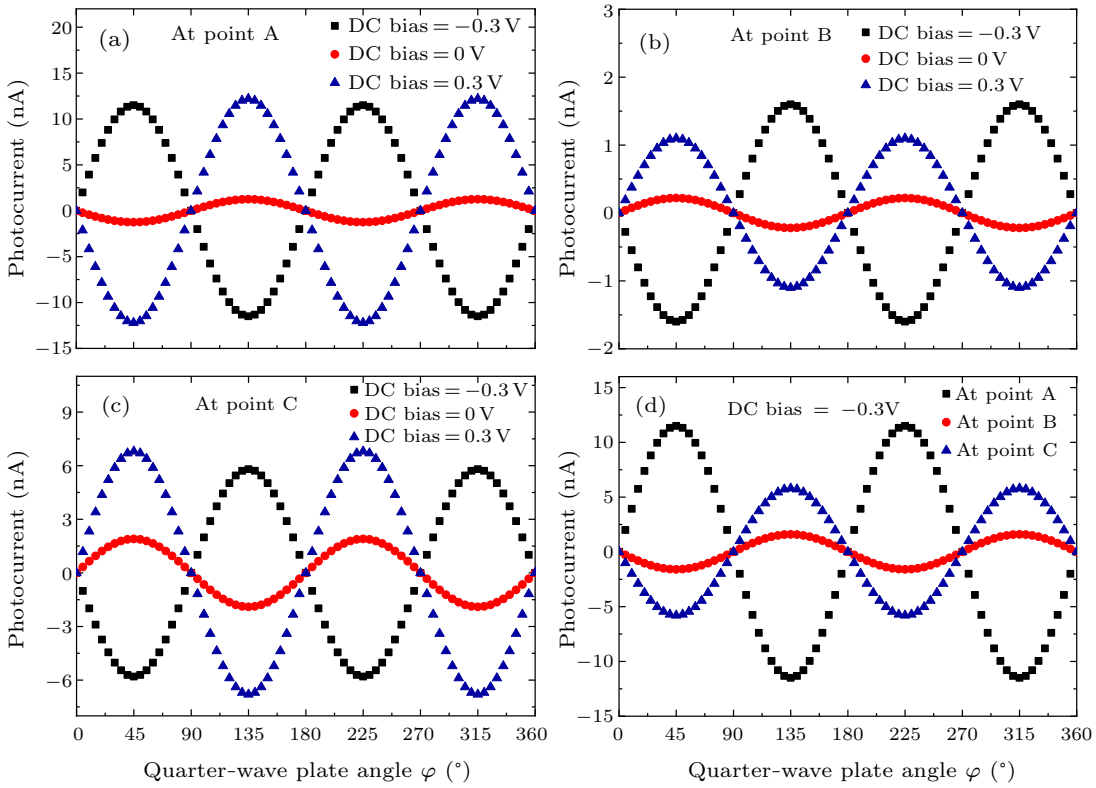


Fig. 2. (a)–(c) HDPC current of the 20-QL sample under different DC biases as a function of the quarter-wave plate angle, i.e., $C\sin(2\varphi)$ component obtained by fitting of Eq. (1) to the experimental data, when the laser is normally illuminated at points A, B, and C, respectively. (d) HDPC current under a DC bias of −0.3 V, i.e., $C\sin(2\varphi)$ component, as a function of the quarter-wave plate, when the laser is illuminated at points A, B, and C, respectively.

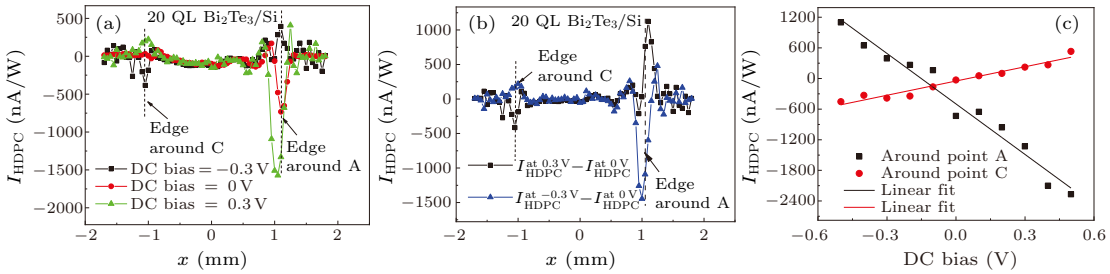


Fig. 3. (a) Dependence of the HDPC current of the 20-QL Bi_2Te_3 film on the light spot position under DC bias of −0.3, 0 and 0.3 V, respectively. (b) HDPC current under 0.3 V and −0.3 V biases, obtained by deducing the HDPC current under zero bias, as a function of light spot position. (c) Dependence of the HDPC current on the DC bias when the laser is vertically illuminated around points A and C, respectively.

points A, B, and C, respectively. It can be seen that the HDPC current at the left edge shows an opposite sign with that on the right edge, due to the fact that the spin helicity of the left edge states is opposite to that of the right edge states.

Figure 3(a) shows the HDPC current as a function of the light spot positions under a DC bias of −0.3 V, 0 V and 0.3 V, respectively, when the laser is moved from the right edge to the left edge of the 20-QL Bi_2Te_3 film. The dashed lines indicate the positions of edge around point A or C. We adopt PEM to replace the quarter-wave plate for this light spot position dependent HDPC measurement. It can be clearly seen that the HDPC current at the edge is much larger than that not on the edge even when the DC bias is zero. By subtracting the HDPC current under zero bias, we can obtain the DC bias dependent HDPC current, as shown in Fig. 3(b). It can be seen that now the HDPC current at the edge under the positive bias shows almost the same amplitude with that under negative bias, and the directions of the HDPC current for the positive and negative biases are opposite. Figure 3(c) shows the dependence of the HDPC current around points A and C on the external applied DC bias, respectively. The solid lines are linear fitting results. It can be seen that the HDPC current at the edge increases almost linearly with DC bias. One may note that the HDPC current measured by using PEM shown in Fig. 3 is larger than that measured by using quarter-wave plate shown in Fig. 2. This is because the light spot position adopted in Fig. 2 may not be the same as that adopted in Fig. 3, since the HDPC currents shown in Figs. 2 and 3 are measured in different measurement systems. Moreover, one can see from Fig. 2 that the HDPC current at point B also increases with DC bias, and it also re-

verses the current direction with the reversal of the DC bias. However, this trend cannot be so obvious in Fig. 3, due to the fact that the HDPC measurement system with a PEM will have larger noise than that with a quarter-wave plate. Since we are mainly focus on the HDPC current on the edge, we still use the PEM in the following experiments, considering that by using PEM, the HDPC current can be measured more quickly and conveniently.

Figures 4(a) and 4(b) show the mapping of the HPDC current as a function of light spot positions under a DC bias of 0.3 V and −0.3 V, respectively. Here, $x = 0$ and $y = 0$ are set at the midpoints of the short and long sides of the sample, respectively. It can be seen that, as the light spot moves around $y = \pm 0.5$ mm, the HDPC current around the edge does not show obvious change, suggesting that the thermoelectric effect has little influence on the HDPC current within this range of position change.

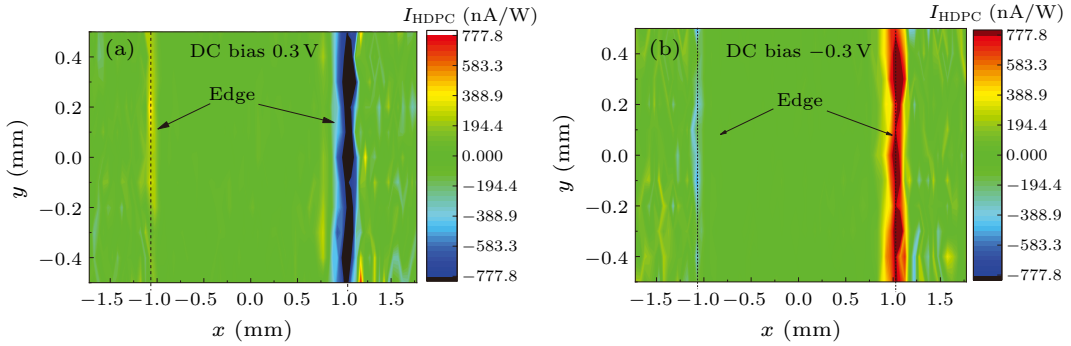


Fig. 4. Mapping of the HPDC current as a function of light spot positions under a DC bias of (a) 0.3 V and (b) −0.3 V, respectively.

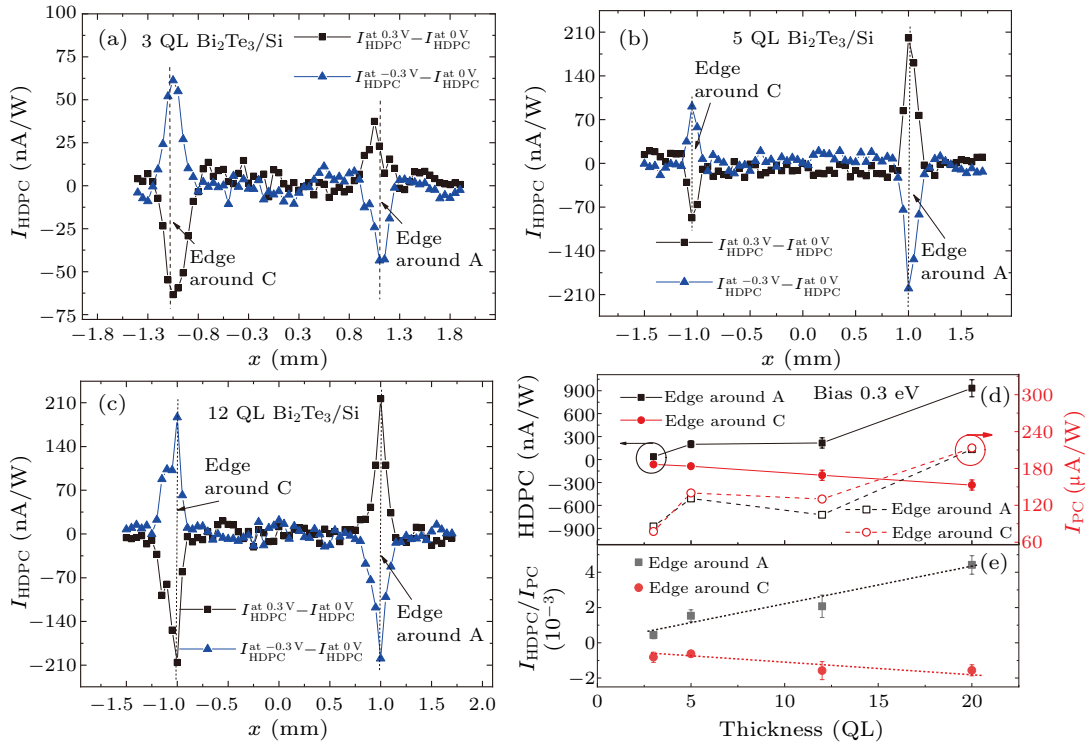


Fig. 5. (a)–(c) Dependence of the HDPC current on the light spot positions under a DC bias of ±0.3 V for the Bi_2Te_3 film of 3, 5, and 12 QL excited by 1064 nm laser, respectively. (d) Dependence of the HDPC current and the photoconductivity current (I_{PC}) around points A and C, respectively, on the thickness of the Bi_2Te_3 film under a DC bias of 0.3 V excited by 1064 nm laser. (e) Dependence of the HDPC current normalized by the photoconductivity current on the thickness of the Bi_2Te_3 film under a DC bias of 0.3 V. The dotted lines are guides for eyes.

Figures 5(a), 5(b), and 5(c) show the dependence of the HDPC current on the light spot positions under a DC bias of ± 0.3 V for the Bi_2Te_3 film of 3, 5, and 12 QL excited by 1064 nm laser, respectively. Here, the HDPC current shown in Figs. 5(a)–5(c) has subtracted the HDPC current under zero bias. It can be seen that the HDPC currents observed in the Bi_2Te_3 film of 3, 5, and 12 QL show similar characteristics with that observed in the 20-QL sample. Figure 5(d) shows the dependence of the HDPC current at the edge around points A and C on the thickness of the the Bi_2Te_3 film under a DC bias of 0.3 V. It can be seen that the HDPC current at the edge increases with the increasing thickness of the Bi_2Te_3 film. Now,

we discuss the reason for this phenomenon. The HDPC current can be expressed as $I_{\mathrm{HDPC}} = eE\Delta NS\mu$. $\Delta N = (n_{\uparrow} - n_{\downarrow})$, which is proportional to the strength of the SOC of the edge states. Here, $n_{\uparrow}$ (or $n_{\downarrow}$) is the density of the photo-generated spin-up (or spin down) carriers; e is the elementary charge; E is the applied electric field; S is the cross sectional area of the current; and μ is the mobility of the photo-generated carriers. With the increase of the film thickness, the width of the current channel increases. As a result, the cross sectional area of the current S will increase, which may lead to the increase of the HDPC current. However, the SOC strength may also change with the film thickness, which will also influence the HDPC current. To discuss this effect, we should first eliminate the influence of the change of channel width on the HDPC current, which can be achieved by normalizing the HDPC current by the common photoconductivity (PC) current. The PC current can be expressed as $I_{\mathrm{PC}} = eENS\mu$, with $N = (n_{\uparrow} + n_{\downarrow})$. Thus, by normalizing the HDPC current with the PC current, we have $I_{\mathrm{HDPC}}/I_{\mathrm{PC}} = \Delta N/N$, which is proportional to the strength of the SOC. Figure 5(e) shows the dependence of the HDPC current normalized by the PC current at the edge around points A and C, respectively, on the thickness of the Bi_2Te_3 film under a DC bias of 0.3 V. The dotted lines are guide for eyes. One can see that the normalized HDPC current almost increases with the film thickness, which is due to the increase of the SOC with the film thickness.

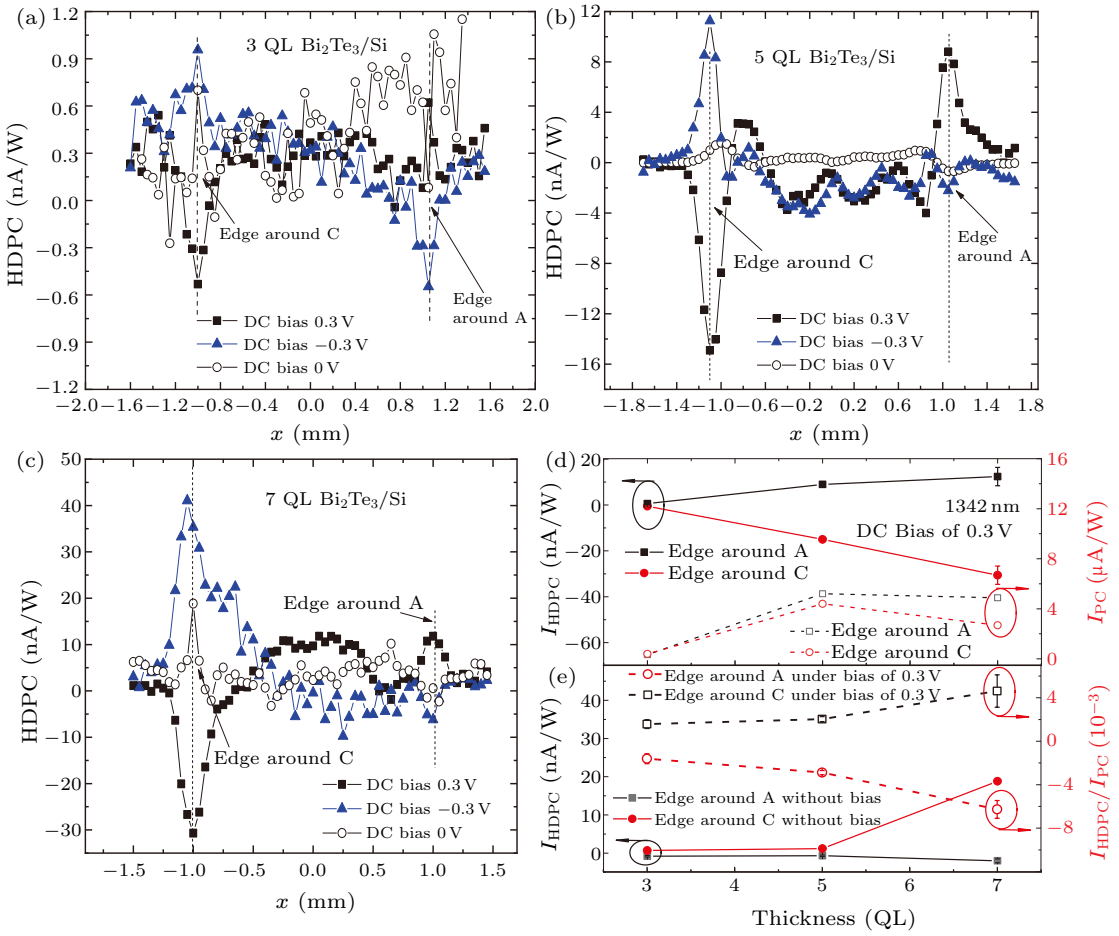


Fig. 6. (a)–(c) Dependence of the HDPC current on the light spot positions under a DC bias of ±0.3 V for the Bi_2Te_3 film of 3, 5, and 7 QL excited by 1342 nm laser, respectively. (d) Dependence of the HDPC current and the PC current around points A and C, respectively, on the thickness of the Bi_2Te_3 film under a DC bias of 0.3 V excited by 1342 nm laser. (e) HDPC current under a DC bias of 0 V and the HDPC current normalized by the PC current under a DC bias of 0.3 V, around points A and C, as a function of the film thickness excited by 1342 nm laser.

Figures 6(a)–6(c) show the HDPC current as a function of light spot positions under a DC bias of ±0.3 V excited by 1342 nm light with a power of 5 mW for the Bi_2Te_3 film of 3, 5, and 7 QL, respectively. Figure 6(d) depicts the dependence of the HDPC current on the thickness of the Bi_2Te_3 film, which indicates that the HDPC current around the edge increases with the thickness of the Bi_2Te_3 film. Figure 6(d) also shows the dependence of the PC current under a DC bias of 0.3 V around points A and C excited by 1342 nm light with a power of 5 mW. By normalizing the HDPC current with the PC current, we find that the normalized HDPC current excited by 1342 nm also increases with the film thickness, as shown in Fig. 6(e). This phenomenon further confirms that the increase of the HDPC current with the film thickness is due to the increase of the SOC of the edge states with the film thickness. It can be seen that the HDPC current excited by 1342 nm light

shows the same characteristics with that excited by 1064 nm light. Therefore, it can be concluded that the HDPC current around the edge does not come from the substrate and it indeed comes from the edge of the Bi_2Te_3 films, since Si substrates can not absorb 1342 nm light and will not generate photocurrent. One may note that the intensity of the HDPC current excited by 1342 nm is about two orders smaller than that excited by 1064 nm light. This can be attributed to the fact that the transition probability excited by 1342 nm is much smaller than that excited by 1064 nm. Here we do not present the HDPC current of the 12-QL and 20-QL Bi_2Te_3 samples excited by 1342 nm, because these two samples are broken after the measurement of the HDPC current excited by 1064 nm.

Theoretically, the HDPC current can be expressed as [18]

$$I_{\mathrm{HDPC}} = \left[\eta P\lambda/(Ahc)\right](\tau_{\mathrm{r}}^{\sigma+} - \tau_{\mathrm{r}}^{\sigma-})e\mu E + \left[k_1\eta P\lambda/(Ahc)\right](\tau_{\mathrm{r}}^{\sigma+} + \tau_{\mathrm{r}}^{\sigma-})e\mu E^2. \quad (2)$$

Here, P is the power of the incident laser, and λ is the wavelength of the laser, A is the area of the laser spot illuminated on the sample, h is Plank's constant, c is the speed of light, k is a constant, η is the optical absorption of the material without applying electric field, μ indicates the mobility of the photo-generated carriers, E is the electric field due to the applied DC bias, $e = 1.6 \times 10^{-19}$ C, $\tau_{\mathrm{r}}^{\sigma+}$ (or $\tau_{\mathrm{r}}^{\sigma-}$) is the lifetime of the photo-generated spin polarized carriers excited by left-handed circularly polarized light σ^+ (or right-handed circularly polarized light σ^-).

The first term on the right-hand side of Eq. (2) strands for the difference between the photoconductivity current induced by left- and right-handed circularly polarized light beams caused by the SOC due to the chiral impurities or defects, since the chiral impurities or defects will lead to $\tau_{\mathrm{r}}^{\sigma+} \neq \tau_{\mathrm{r}}^{\sigma-}$. The second term in Eq. (2) represents the helicity dependent photoconductivity current due to the spin polarization induced by electric field or due to the spin Hall conductance effect.[16] In our experiments, we mainly observe the HDPC current that shows a linear dependence on external electric field, suggesting that the HDPC is mainly due to the chiral impurities or defects at the edges. We do not observe the HDPC current that is proportional to E^2, which may be because this effect is weak and the resulting photocurrent is so small that it submerges in the noise.

Actually, the intrinsic SOC of the edge states can also lead to the HDPC current, which can be understood in the following way. Firstly, since the left and right edge states have opposite spin helicities, as shown in Fig. 7(a), under the excitation of circularly polarized light, optical transitions of SS1→SS2 and CB1→SS2 will occur, leading to unbalanced distributions of photo-generated carriers in k space, as shown in Fig. 7(b). Here, SS1 and SS2 indicate the first and second surface states, respectively. CB1 denotes the first conduction band. Due to the opposite spin helicities of the left and right edge states, under zero bias, the left and right edge states will generate photocurrent flowing in opposite directions. This phenomenon has been clearly observed in our experiments, which is shown in Figs. 2 and 6(e). Under a DC bias, this HDPC current will be amplified by the electric field, and it reverses the sign with the reversal of the electric field.

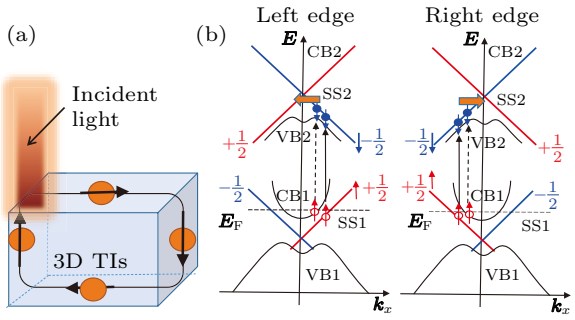


Fig. 7. (a) Schematic drawing of the spin direction of the electrons on the left and right edges as well as that on the top and bottom surfaces of 3D TIs. (b) Schematic illustration of the optical transitions excited by circularly polarized light for the electrons on the left and right edges, respectively. The solid and dashed vertical lines indicate the transitions of electrons from the first surface states (SS1) to the second surface states (SS2), and from the first conduction band (CB1) to the SS2, respectively.

It is worth mentioning that the electrons on the edge states have spin directions that are parallel or antiparallel to the incident direction of the circularly polarized light. Thus, according to the optical transition selection rule of point group C_{3v},[23] to which the surface states of 3D TIs belong, these electrons will absorb the light and jump to higher energy levels, and thus generate photocurrent. However, for the top and bottom surface states, most of the electrons have spin directions that are perpendicular to the incident direction of the light, and they will not absorb the light according to the optical selection rules. The observed photocurrent when the light is incident at point B mainly comes from the spin polarized carriers with an out-of-plane spin due to the hexagonal warping effect of Bi_2Te_3.[24] Since this effect is weak, the observed HDPC current at point B is smaller than that observed at the edges.

4. Conclusion

In summary, we have investigated the helicity-dependent photoconductivity current of the edge states in three-dimensional topological insulator Bi_2Te_3 films of different thicknesses excited by 1064 nm and 1342 nm laser. It is found that the HDPC current on the left edge of the Bi_2Te_3 film shows an opposite sign with that on the right edge, and the HDPC current reverses its direction with the reversal of the longitudinal electric field. The HDPC current around the edge increases almost linearly with the increasing longitudinal electric field, and it also increases with the thickness of the Bi_2Te_3

films, which is due to the increases of the SOC of the edge states with the film thickness. The HDPC current excited by 1342 nm shows the same characteristics as those excited by 1064 nm light, but the intensity of the HDPC current excited by 1342 nm is about two orders smaller than that excited by 1064 nm light, which may be attributed to much smaller transition probability when excited by 1342 nm. By theoretical analysis, we find that the HDPC current observed in this work may come from the intrinsic SOC or the SOC introduced by the chiral impurities or defects. This work provides a method of using HDPC to investigate the edge states in 3D TIs.

Acknowledgments

We thank Professor Ke He and Kejing Zhu for providing the samples and useful discussions.

Project supported by the National Natural Science Foundation of China (Grant Nos. 62074036 and 61674038) and the National Key Research and Development Program of China (Grant No. 2016YFB0402303).

References

[1] Frolov A S, Usachov D Y, Fedorov A V, Vilkov O Y, Golyashov V, Tereshchenko O E, Bogomyakov A S, Kokh K, Muntwiler M, Amati M, Gregoratti L, Sirotina A P, Abakumov A M, Sanchez-Barriga and Yashina L V 2022 *Acs Nano* **16** 20831

[2] Nikoofard H, Esmaeilzadeh M, Farghadan R and Sun J T 2022 *Phys. Rev. B* **106** 165127

[3] Thanopulos I, Yannopapas V and Paspalakis E 2022 *Opt. Lett.* **47** 5240

[4] Yu R, Cao J F, Meng X Y, Zhu F Y, Li J Q, Qu G X, Huang Y B, Wang Y and Tai R Z 2022 *ACS Appl. Mater. Inter.* **14** 48171

[5] Brito D, Pérez-Rodriguez A, Khatri I, Tavares C J, Amado M, Castro E, Diez E, Sadewasser S and Claro M S 2022 *J. Appl. Phys.* **132** 115107

[6] Li M, Yu J, Cui G, Chen Y, Lai Y, Cheng S and He K 2022 *J. Appl. Phys.* **131** 113902

[7] Bai Y, Li N, Li R and Liu P 2022 *Adv. Phys. X* **7** 2013134

[8] Chen Y L, Analytis J G, Chu J H, Liu Z K, Mo S K, Qi X L, Zhang H J, Lu D H, Dai X, Fang Z, Zhang S C, Fisher I R, Hussain Z and Shen Z X 2009 *Science* **325** 178

[9] Sharma S, Kumar S, Kumar A, Shimada K and Yadav C S 2022 *J. Appl. Phys.* **132** 105108

[10] Lv B, Qian T and Ding H 2019 *Nat. Rev. Phys.* **1** 609

[11] Segev M and Bandres M A 2021 *Nanophotonics* **10** 425

[12] Chong S K, Liu L, Watanabe K, Taniguchi T, Sparks T D, Liu F and Deshpande V V 2022 *Nat. Commun.* **13** 6386

[13] Rojas-Sanchez J C, Oyarzun S, Fu Y, Marty A, Vergnaud C, Gambarelli S, Vila Laurent, Jamet M, Ohtsubo Y, Taleb-Ibrahimi A, Le Fevre P, Bertran F, Reyren N, George J M and Fert A 2016 *Phys. Rev. Lett.* **116** 096602

[14] Jamali M, Lee J S, Jeong J S, Mahfouzi F, Lv Y, Zhao Z, Nikolic B K, Mkhoyan K A, Samarth N and Wang J P 2015 *Nano Lett.* **15** 7126

[15] Pan Y, Wang Q Z, Yeats A L, Pillsbury T, Flanagan T C, Richardella A, Zhang H, Awschalom D D, Liu C X and Samarth N 2017 *Nat. Commun.* **8** 1037

[16] Seifert P, Vaklinova K, Ganichev S, Kern K, Burghard M and Holleitner A W 2018 *Nat. Commun.* **9** 331

[17] Taskin A A and Ando Y 2009 *Phys. Rev. B* **80** 085303

[18] Yu J, Zhuang H, Zhu K, Chen Y, Liu Y, Zhang Y, Yin C, Cheng S, Lai Y, He K and Xue Q K 2021 *Phys. Rev. B* **104** 045428

[19] McIver J W, Hsieh D, Steinberg H, Jarillo-Herrero P and Gedik N 2011 *Nat. Nanotechnol.* **7** 96

[20] Yu J, Zeng X, Zhang L, He K, Cheng S, Lai Y, Huang W, Chen Y, Yin C and Xue Q 2017 *Nano Lett.* **17** 7878

[21] Chis V, Sklyadneva I Y, Kokh K A, Volodin V A, Tereshchenko O E and Chulkov E V 2012 *Phys. Rev. B* **86** 174304

[22] Mei F H, Tang N, Wang X Q, Duan J X, Zhang S, Chen Y H, Ge W K and Shen B 2012 *Appl. Phys. Lett.* **101** 132404

[23] Ganichev S D and Prettl W 2003 *J. Phys.: Condens. Matter* **15** R935

[24] Huang Y Q, Song Y X, Wang S M, Buyanova I A and Chen W M 2017 *Nat. Commun.* **8** 15401